PROCEEDINGS OF SPIE

SPIEDigitalLibrary.org/conference-proceedings-of-spie

Co₂MnSi:Pt multilayers for giant spin Seebeck devices

Christopher Cox
Andrew J. Caruana
Michael D. Cropper
David M. Tatnell
Christy J. Kinane
Timothy R. Charlton
Kelly Morrison

SPIE.

Co_2MnSi:Pt multilayers for giant spin Seebeck devices

Christopher Cox*[a], Andrew J. Caruana[a,b], Michael D. Cropper[a], David M. Tatnell[a], Christy J. Kinane[b], Timothy R. Charlton[b,c], Kelly Morrison[a].

[a] Physics, Loughborough University, Loughborough, Leicestershire, LE11 3TU, United Kingdom; [b] ISIS Neutron and Muon Source, STFC Rutherford Appleton Laboratory, Harwell Science and Innovation Campus, Oxon OX11 0QX, United Kingdom; [c] Thin Films and Nanostructures in Quantum Condensed Matter Division, Oak Ridge National Lab, Oak Ridge, TN 37831

*c.d.w.cox@lboro.ac.uk

ABSTRACT

The spin Seebeck effect (SSE) has been widely studied as a potential mechanism for energy harvesting. However, the efficiency of such devices, utilizing the spin thermoelectric effect in thin film form, has not yet reached a sufficient value to make them economically viable. It is therefore imperative that advances are made to investigate means by which the thermoelectric signal can be enhanced. Multilayers of Co_2MnSi and Pt are fabricated and characterized in an attempt to observe enhanced voltages. We report that bilayers of ferromagnetic conductor/normal metal (FM/NM) exhibit a Longitudinal SSE response and that repetitive stacking of such bilayers results in an increased thermoelectric voltage that is highly dependent upon the quality of CMS/Pt and Pt/CMS interfaces.

Keywords: Heusler Alloys, Spintronics, Spin Seebeck Effect, Thin Films, Pulsed Laser Deposition, Anomalous Nernst Effect, Interfaces

1. INTRODUCTION

Thermoelectric generation – the conversion of heat into useful voltage – is a well-established field of research that is however plagued by limitations on the efficiency of potential devices. As useful power will be controlled by (a) the figure of merit zT, and (b) the magnitude of the temperature difference, ΔT, that can be maintained across the device, conventional thin film thermoelectrics (based on the transfer of charges alone), are rarely considered economically viable due to a combination of lower efficiencies and power generation. The emergence of the field of spin caloritronics[1–6] provides a potential gateway for change that could see this perception of thermoelectrics challenged. In spin caloritronics the manipulation of both the charge and spin of the electrons within a magnetic material can provide a possible enhancement of the efficiency of thin film thermoelectrics. For example, alternative thermoelectric generators based on the spin Seebeck effect (SSE), as shown in figure 2(a), would see the electric and thermal conductivities (the bottlenecks of conventional thermoelectric materials) decoupled.

The spin Seebeck effect is the generation of a spin polarized current in a magnetized material that is subjected to a temperature gradient. Magnetic materials investigated so far include metals and insulators with a range of magnetic ordering from ferromagnetic[7–11] to antiferromagnetic[12], where significant emphasis has been placed on investigation of magnetic insulators such as YIG[9,13–15]. Of particular interest are half metallic ferromagnets (HMF): materials which can act as an insulator for one spin state and a conductor for the other. Two conditions must be satisfied for this HMF state to occur: firstly there must be a band gap in the density of states (DOS) of the minority spin state; secondly the Fermi level should be located within this bandgap. The existence and location of this bandgap is highly dependent upon the materials structural properties.

Co_2MnSi (CMS), a member of the full Heusler family of alloys, has been identified as one of these HMF with a 100% spin polarization (σ)[16]. In the case of thermoelectric generation the value of this σ represents a material's ability to produce a fully spin polarized current and in this case, by way of the SSE. However, detection of this spin polarization using non-local spin valves has shown that the interface between the CMS and the spin 'sink' material, in our case Pt, is crucial to achieving this 100% σ in devices[17]. The structural properties have also been found to determine the spin polarization of Co_2MnSi with a reduced value of 89% found for CMS/AlOx films even in the $L2_1$ with poor interface quality subject to Al diffusion into the CMS[18]. A detailed investigation of the effect of Ag diffusion into the CMS film

Spintronics X, edited by Henri-Jean Drouhin, Jean-Eric Wegrowe, Manijeh Razeghi, Henri Jaffrès, Proc. of SPIE
Vol. 10357, 1035731 · © 2017 SPIE · CCC code: 0277-786X/17/$18 · doi: 10.1117/12.2271303

showed that σ is compromised within 1 to 2 atomic layers of the CMS due to Ag substitution of Si[19]. From this evidence it can be assumed that the introduction of disorder from site-swapping or anti sites, not only at the interface but within the bulk of the film, can significantly affect σ and consequently reduce the potential spin injection from CMS into Pt.

Many of the ternary Heusler alloys studied previously have displayed transitions from disordered to ordered structures as a function of deposition or annealing temperature[20–22]. Complete disorder (classed as A2) results from disorder on the Co, Mn and Si sites. B2 disorder requires ordered Co lattices and allows Mn-Si disorder. $L2_1$ order denotes order on the sites. Figure 1 provides images of the unit cell for each of the 3 phases described above, shifted by $\frac{a_1}{4}$ for clarity where a_1 is the lattice parameter. With Co_2MnSi having such a high theoretical σ, it is an ideal candidate for the FM layer in a SSE device.

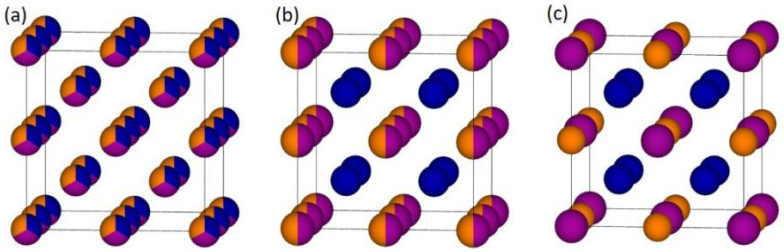

Figure 1 Representation of Co_2MnSi unit cell shifted by $a_1/4$ to observe the 8 stacked bcc lattices. (a) A2 order (b) B2 order (c) $L2_1$ order. Co (Blue), Mn (Purple) and Si (Orange) are situated on the (¼, ¼, ¼), (0, 0, 0) and (½, ½, ½) atomic positions in the fully ordered $L2_1$ unit cell.

To measure the spin Seebeck effect, a thin layer of Pt (or other material with a large spin Hall angle such as beta-W[23] or Ta[24]) is deposited on top of the material to be investigated. The application of a thermal gradient will generate a spin current that is then injected into this Pt layer. Spin dependant scattering – the inverse spin Hall effect (ISHE) – will then result in a measurable voltage across the sample, as shown in figure 2(a).

Other magnetothermal effects need to be considered, however, when performing spin Seebeck measurements. For example, the Nernst effect (NE) is another phenomenon that arises when a conductor is subjected to a temperature gradient. Here, as carriers drift from one end of the conductor to another, spin dependant scattering results in a generation of an electric field established from the cross product of B_x and ΔT_z. In magnetic materials, the NE becomes the anomalous Nernst Effect (ANE) due to the additional contribution of the material's own magnetization to the spin dependant scattering. Therefore, in magnetic conductors subjected to a temperature gradient, alongside the spin Seebeck effect is the ANE (see figure 2(b)). As a thin layer of Pt is often chosen to observe the SSE, there is also the possibility of a proximity induced magnetism (and hence ANE) in the Pt layer, which is expected to decrease sharply as the Pt thickness is increased. Historically, the ANE has been difficult to separate from the longitudinal SSE (LSSE) due to similar measurement geometries.

With regards to the use of the SSE for energy harvesting, this technique would require generation of significant amounts of voltage, compared to the microvolts typically observed for single contacts. More recently, Ramos et al demonstrated that multilayer $[Fe_3O_4{:}Pt]_n$ grown on MgO exhibited significant enhancement of the observed SSE[25]. Lee et al also discovered a similar increase in the thermoelectric voltage in $[CoFeB/Pt]_n$ multilayers grown on Si[26]. This suggests a potential improvement in the thermoelectric voltage for a wide range of material systems and here we present data on $[Co_2MnSi/Pt]_n$ multilayers - where now we observe a metal:metal multilayer stack – deposited on glass substrates. We focus in particular on the impact of structural disorder and the interface on the SSE voltage measured.

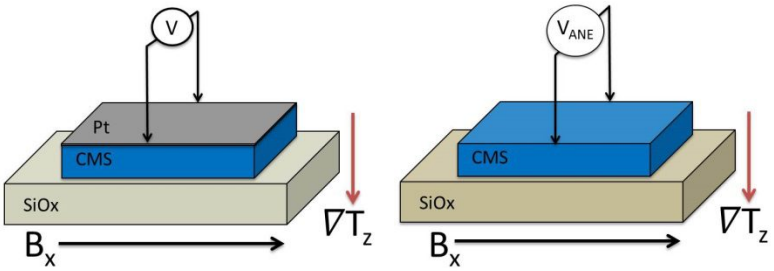

Figure 2 (a) Spin Seebeck measurement geometry and (b) ANE measurement geometry.

2. EXPERIMENTAL DETAILS

2.1 Fabrication

The films produced in this paper were deposited under UHV (base pressure of $5x10^{-9}$ mbar) by Pulsed Laser Deposition (PLD) using a Nd:YAG solid state laser (λ = 1064 nm) operating at a repetition rate of 10 Hz. The primary beam was frequency doubled to 532nm before entering an optics arrangement to filter out infrared and ultraviolet wavelengths. The beam then passed through a mask (selecting 90% of the beam profile) before entering the chamber and striking the target. The targets used here were Co_2MnSi and Pt (Pi-Kem 99.9 % purity). Glass (SiO_2) substrates were explored as an alternative to expensive single crystals such as GaAs[27–31], $MgAlO_3$[32] and MgO[16,33,34] which have been used heavily across the literature because of the small lattice mismatch between the Co_2MnSi and substrates. In an effort to reduce the deposition temperature of the FM layer (Co_2MnSi), seed layers are often used to promote textured growth on amorphous substrates however because of the multilayer architecture in this work, direct contact between the CMS and Pt is needed for good spin current injection.

Prior to deposition, the substrates were outgassed at 400°C (to remove surface contamination) before passive cooling to the deposition temperature, T_{Dep}= 170° C. This deposition temperature was chosen as the threshold of good crystalline growth, as discussed in more detail in[35]. The Pt in the multilayers was deposited at room temperature after cooling the substrate from 170° C. Annealing of the multilayers took place *in-situ* after deposition of the whole stack was complete. A summary of the films investigated in this study is given in Table 1 (CMS optimization) and Table 2 (Multilayers).

Table 1 Table of samples investigated here, where T_{Dep} was the deposition temperature and T_{Ann} was the annealing temperature. The bulk value of the lattice parameter a_1 is 5.654 nm[36].

Composition	T_{Dep} (°C)	T_{Ann} (°C)	Order	a_1(nm)
SiO_2/Co_2MnSi	170	-	A2	5.736
SiO_2/Co_2MnSi	170	100	A2	5.687
SiO_2/Co_2MnSi	170	300	B2	5.675
SiO_2/Co_2MnSi	170	450	$B2/L2_1$	5.634

2.2 Analysis

For structural analysis, X-Ray diffraction patterns for all samples were obtained on a Bruker D2 Phaser (Cu Kα λ=1.54nm). Grazing incidence XRD (GIXRD) patterns and X-Ray Reflectivity (XRR) curves were taken using a Siemens D5000 with the diffracted beam optics consisting of Soller Slits and LiF crystal for GIXRD and 0.05mm receiving slit, 0.6mm anti-scatter slit, 0.1mm detector slit, and a graphite monochromator for XRR. A scintillation point detector was used for both techniques. Polarized Neutron Reflectometry (PNR) was performed (as a complementary technique to XRR) to obtain the structural and magnetic profile as a function of depth. PNR was performed on the Polref beamline at ISIS Neutron Source (Harwell, UK).

Room temperature resistivity was obtained by the Van Der Pauw technique using a Keithley 6221/2182A current source (probe current of 0.1 mA) and nanovoltmeter in conjunction with a K181 switch system. The resistivity, ρ, was calculated from the sheet resistance, R_s, along with the thickness obtained by XRR.

The anomalous Nernst (ANE) and spin Seebeck effect (SSE) contributions were measured using an in-house constructed system. The set up used 2 Peltier cells (one acting as a heat source and the other as a heat flow monitor), type E

thermocouples to measure the temperature difference across the sample and a Keithley nanovoltmeter 2182A to measure the voltages generated (V_{ANE}+V_{SSE}). A more detailed overview of the technique can be found in [8]. The ANE contributions from single layer CMS films was measured as well as control samples (deposited with Pt) to estimate the contribution to the observed voltage from the ANE. The spin Seebeck coefficient used to normalize these measurements was defined as follows $S_{dT} = V_{ISHE}/(\Delta T\, L_y)$ or according to Sola *et al.*[37] $S_{VQ} = (V_{ISHE}\, A_t)/(V_Q\, L_y)$, where L_y and ΔT are the contact separation and temperature difference detected by the thermocouples. In the latter equation, A_t is the thermal contact area between the sample and the Peltier cells (in our case 4.84x10^{-4} m^2) and V_Q is the heat flow calculated from the voltage measured by the second calibrated Peltier cell, allowing for a sensor dependent factor.

3. DATA

3.1 Characterization of Co_2MnSi films

Prior to commencing the deposition of multilayers, a thorough optimization of the deposition parameters was carried out[35]. This work and others found that crystalline growth began to occur at T_{Dep} = 170°C. These films however, initially formed in the disordered A2 state (Co-Mn-Si site swapping); the films were subsequently annealed at 450°C[16,38–40] to promote $L2_1$ ordering (good order on all sites) or 300°C to investigate B2 ordering (Mn-Si disorder) found at this temperature.

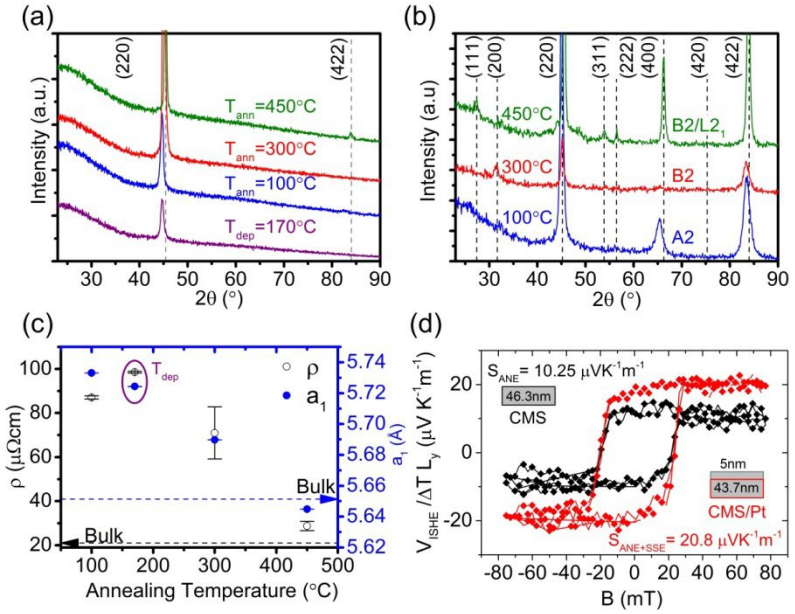

Figure 3 Structural and electrical characterization of Co_2MnSi thin films. (a) XRD shows textured [220] growth out of plane, (b) GIXRD shows the progression of order with increasing T_{ann}. (c) resistivity, ρ, (left axis) and lattice parameter, a_1 (right axis) as a function of T_{Ann}, indicate convergence on bulk values as T_{Ann} is increased, and (d) CMS and CMS/Pt thermoelectric signals as a function of applied magnetic field show clear field response due to ANE and SSE.

Figures 3(a) and 3(b) show typical out of plane XRD and GIXRD for these samples. It is clear from figure 3(a) that the films all exhibited strong (220) out of plane texture; all other expected peaks were absent. In order to characterize the order of these films, GIXRD was used to look at the lattice planes that are not parallel to the film surface, shown in figure 3(b). Here it can be seen that films annealed at 100°C showed the (220), (400) and (422) reflections that indicate A2 disorder. As the annealing temperature was increased to 300°C the (200) peak appeared, suggestive of B2 order. Upon a further increase to 450°C, all peaks indicative of $L2_1$ order were present. Figure 3(b) also hints at a small amount of segregation represented by the appearance of a low and high angle shoulder on the (220) peak at 450°C. These peaks belong to the Co(111) reflection and MnSi alloys respectively.

Another identifier, as to the degree of ordering, lies in the resistivity of the films, as shown in figure 3(c). Here, the resistivity of as deposited films (and those annealed at 100°C) was of the order of ρ~100 μΩ cm. This converged upon

the bulk value of 21 μΩ cm[41] as the films became more ordered at 450°C. Also shown in figure 3(c) is the lattice parameter, a_1, calculated from the position of the (220) peaks in figure 3(a). The value of a_1 was larger than the bulk value of 5.654Å[36] for the film annealed at 100°C and decreased as the annealing temperature was increased, eventually converging on the bulk value. The appearance of superstructure peaks, decreasing resistivity and decreasing a_1 all indicate an increase in order with annealing temperature[42].

In order to quantify the contribution of the ANE signal to the observed thermoelectric voltage a set of control samples were fabricated. These consisted of 40nm thin films of CMS deposited by PLD, where the ANE signal was measured from the surface of one film (t_{CMS} = 46.3nm). On the second sample (t_{CMS} = 43.7nm), a 5nm Pt contact layer was deposited on top of the Co_2MnSi film using a Quorum Q150T sputter coater at a typical pressure of $5x10^{-3}$ mbar. The ANE and SSE contributions measured for these samples are shown in figure 3(d). It can be seen that the observed voltage doubled from 10.25 μV K^{-1} m^{-1} to 20.8 μV K^{-1} m^{-1} with the addition of the Pt layer.

3.2 Characterization of multilayers

The data presented here corresponds to the implementation of the optimized CMS films into multilayer spin Seebeck effect devices. Multilayers (ML's) were fabricated and then annealed at 300° C or 450° C for 1 hour. A summary of the films investigated in this study are presented in table 2.

Table 2 Table of multilayer samples where T_{Dep} is the deposition temperature and T_{Ann} is the annealing temperature. Order is estimated from GIXRD patterns.

Composition	T_{Dep} (°C)	T_{Ann} (°C)	Order
$SiO_2/Co_2MnSi/Pt$	170/RT	300	B2
$SiO_2/Co_2MnSi/Pt$	170/RT	450	$L2_1$
$SiO_2/[Co_2MnSi/Pt]_2$	170/RT	300	B2
$SiO_2/[Co_2MnSi/Pt]_2$	170/RT	450	$L2_1$
$SiO_2/[Co_2MnSi/Pt]_3$	170/RT	300	B2
$SiO_2/[Co_2MnSi/Pt]_3$	170/RT	450	$L2_1$

Structural analysis of the ML's can be seen in figure 4. GIXRD (figure 4(a) and 4(b)) shows that for a single bilayer, the CMS formed in the B2 structure with the polycrystalline Pt displaying a large amount of strain signified by broad peaks. At a temperature of 300° C, annealing promoted B2 order (figure 4(a)) in the majority of the films. Annealing at 450° C, figure 4(b) shows GIXRD, where, it can be seen that for all films, n=1-3, the CMS films contained $L2_1$ ordering indicated by the presence of the CMS (111) peak. The Pt was also well formed with a strong (111) and (222) reflection. However, it can be clearly seen that there is significant alloying of the components of the CMS and Pt indicated by (*).

Polarized Neutron Reflectometry (PNR) provided insight into the magnetic structure as a profile of depth (z). Figure 4(c) displays PNR data for single bilayers. Damping of the Kiessig fringes for the sample annealed at 450° C indicates a diffusive interface (inset). Inter-diffusion and morphological roughness are indistinguishable using PNR, however we can assume that as the 2 samples underwent the same treatment prior to annealing, that the roughness is chemical i.e. inter-diffusion. As a result of a diffuse interface i.e. the substitution of Pt into the CMS lattice, the magnetism, in these areas at least, is compromised, indicated by an increased interface in the magnetic scattering length density profile (which is dependent upon the magnetization of the material).

Comtesse *et al.* found that the magnetism and density of states of certain Heusler alloys containing Co is highly dependent on the lengths of the nearest neighbor bonding of the Co-Mn[43]. Co and Mn would ordinarily couple antiferromagnetically in the binary alloy, CoMn, however with the reduced distance when the bond is in the ternary alloy (CMS), the interaction is positive forming FM coupling. It is by the breakdown of this mechanism that when the Pt either replaces either of the two atoms, forming a weak if not null interaction or the presence of the Pt alters the separation distance of the Co and Mn forcing the interaction to become negative destroying the band gap in the DOS and destroying the spin polarization a the interface, restricting spin current injection into the Pt.

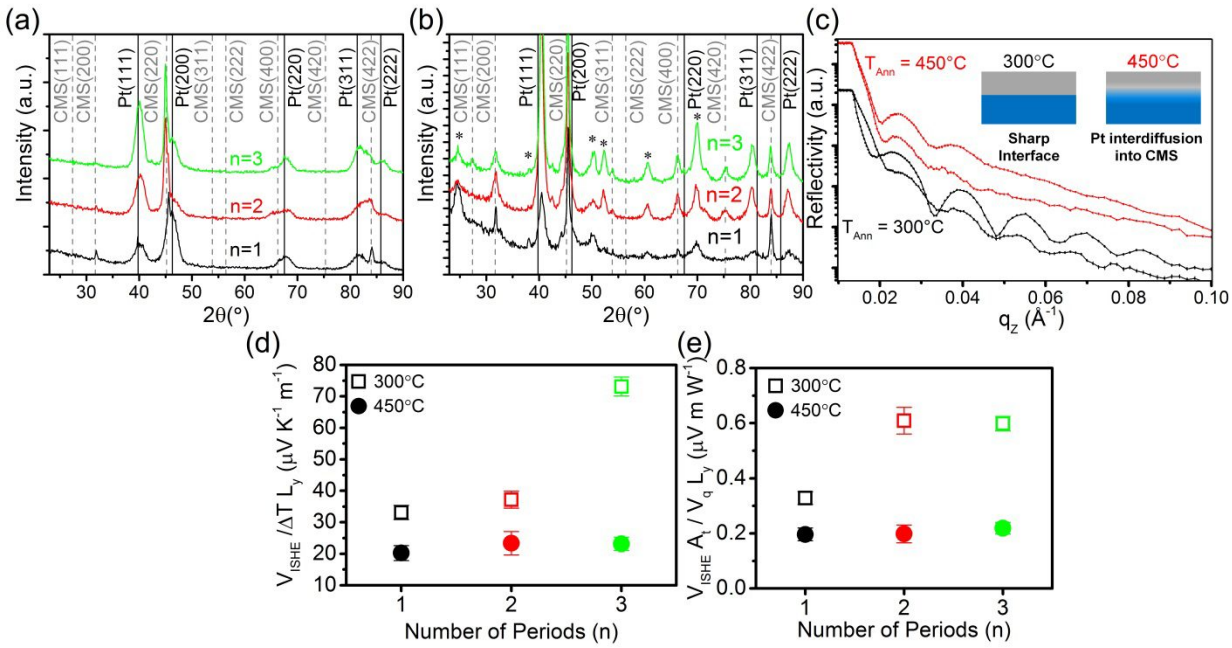

Figure 4 GIXRD patterns for multilayer films annealed at (a)300° C and (b) 450° C. Alloying is clearly present in (b) indicated by (*). (c) Polarized neutron reflectometry taken on the Polref beamline at (RAL, Oxford) for single bilayers annealed at 300° C and 450° C. (d) and (e) SSE measurements of $[Co_2MnSi/Pt]_n$ ML's represented as a function of temperature difference, ΔT, between the hot and cold sides of the sample and as a function of heat flow across the thermal contact area, A_t, respectively.

Figure 4(d) and 4(e) show the spin Seebeck coefficients calculated as a function of both ΔT and V_Q. Comparing films annealed at 300° C and 450° C across all n, one can clearly see the impact the alloying at the interfaces has upon the V_{ISHE}. The significantly lower voltage observed in ML's annealed at 450° C can be attributed to the reflection of the spin current at the diffuse CMS/Pt interface reducing the spin mixing conductance. This can be applied to the n=2 and n=3 MLs annealed at 450° C preventing the propagation of spin currents through the CMS/Pt/CMS interfaces. It is assumed therefore that any layers below the terminating bilayer do not inject the proposed spin current into the top layer. Hence, as the voltages observed across n=1-3 for T_{Ann}= 450° C are relatively constant, only the topmost bilayer can be considered to be contributing to the V_{ISHE}.

However, in ML's annealed at 300° C, the lack of inter-diffusion is beneficial to spin transport across the CMS/Pt/CMS interface and an increase in the V_{ISHE} is observed from n=1 to n=3 as a function of both ΔT and V_Q.

4. CONCLUSION

The growth and quality of a Co_2MnSi thin film is highly dependent upon fabrication technique, target stoichiometry and substrate not to mention deposition temperature and annealing methods. Whereas before most work has been focused on GaAs as a well lattice matched substrate, the use of glass in this study complicates the substrate/Co_2MnSi interface due to strain caused by the lack of seeding lattice parameter. Initial characterization of the CMS films took place and in the first instance it can be seen that crystalline films of Co_2MnSi can be grown at 170° C on amorphous substrates with an out of plane (220) texture. Additional information supplied by GIXRD confirmed that the annealing process formed larger grains and more ordered films as the temperature was increased to 300° C (B2) and 450° C ($L2_1$) in good agreement with previous studies on this crystal system[40]. The ANE contribution from the FM layer has been found to be approximately half of the total thermoelectric signal from a FM/NM bilayer.

Interestingly, when these temperatures were used as starting parameters to fabricate multilayer heterostructures, magnetically dead layers at the interfaces formed at both temperatures leading to significant alloying between Pt and CMS, observable in XRD. It was observed however that annealing the stack at 300° C reduced the thickness of the

magnetic dead-layers at the interfaces meaning that inter-diffusion (seen at the higher temperature) was more controlled compared to stacks annealed at 450° C. Evidence of the phase separation and inter-diffusion manifested itself as a reduction in the thermoelectric voltage across the multilayer series. To understand this reduction of V_{ISHE} with higher annealing temperatures, one can take the view that the spin mixing conductance, $g^{\uparrow\downarrow}$, at the interface is reduced when significant intermixing of the Co_2MnSi and Pt is present. This reduces the effective spin current injected into the Pt resulting in the reduced V_{ISHE}.

To summarize this work, the V_{ISHE} observed from $[Co_2MnSi/Pt]_n$ ML's has been shown to increase with the number of repetitions, up to n=3, in line with previous finding from FM/NM ML's[25,26]. Providing more evidence for the proposed Giant spin Seebeck Effect.

References

[1] Goennenwein, S. T. B.., Bauer, G. E. W., "Spin caloritronics: Electron spins blow hot and cold," Nat. Nanotechnol. **7**(3), 145–147 (2012).

[2] Uchida, K., Xiao, J., Adachi, H., Ohe, J., Takahashi, S., Ieda, J., Ota, T., Kajiwara, Y., Umezawa, H., et al., "Spin Seebeck insulator," Nat. Mater. **9**(11), 894–897 (2010).

[3] Johnson, M.., Silsbee, R. H., "Thermodynamic analysis of interfacial transport and of the thermomagnetoelectric system," Phys. Rev. B **35**(10), 4959–4972 (1987).

[4] Flipse, J., Dejene, F. K., Wagenaar, D., Bauer, G. E. W., Youssef, J. Ben., van Wees, B. J., "Observation of the Spin Peltier Effect for Magnetic Insulators," Phys. Rev. Lett. **113**(2), 27601 (2014).

[5] Bauer, G. E. W., Saitoh, E.., van Wees, B. J., "Spin caloritronics," Nat. Mater. **11**(5), 391–399 (2012).

[6] Boona, S. R., Myers, R. C.., Heremans, J. P., "Spin caloritronics," Energy Environ. Sci. **7**(3), 885 (2014).

[7] Uchida, K., Nonaka, T., Kikkawa, T., Kajiwara, Y.., Saitoh, E., "Longitudinal spin Seebeck effect in various garnet ferrites," Phys. Rev. B **87**(10), 104412 (2013).

[8] Morrison, K., Caruana, A. J.., Cox, C., "Towards a standard spin Seebeck measurement," arXiv, 1705.02491 (2017).

[9] Uchida, K., Adachi, H., Ota, T., Nakayama, H., Maekawa, S.., Saitoh, E., "Observation of longitudinal spin-Seebeck effect in magnetic insulators," Appl. Phys. Lett. **97**(17), 172505 (2010).

[10] Uchida, K., Takahashi, S., Harii, K., Ieda, J., Koshibae, W., Ando, K., Maekawa, S.., Saitoh, E., "Observation of the spin Seebeck effect," Nature **455**(7214), 778–781 (2008).

[11] Bosu, S., Sakuraba, Y., Uchida, K., Saito, K., Ota, T., Saitoh, E.., Takanashi, K., "Spin Seebeck effect in thin films of the Heusler compound Co2MnSi," Phys. Rev. B **83**(22), 224401 (2011).

[12] Ohnuma, Y., Adachi, H., Saitoh, E.., Maekawa, S., "Spin Seebeck effect in antiferromagnets and compensated ferrimagnets," Phys. Rev. B **87**(1), 14423 (2013).

[13] Siegel, G., Prestgard, M. C., Teng, S.., Tiwari, A., "Robust longitudinal spin-Seebeck effect in Bi-YIG thin films.," Sci. Rep. **4**, 4429 (2014).

[14] Kehlberger, A., Jakob, G., Onbasli, M. C., H. Kim, D., Ross, C. a.., Kläui, M., "Investigation of the magnetic properties of insulating thin films using the longitudinal spin Seebeck effect," J. Appl. Phys. **115**(17), 17C731 (2014).

[15] Kikkawa, T., Uchida, K., Shiomi, Y., Qiu, Z., Hou, D., Tian, D., Nakayama, H., Jin, X.-F.., Saitoh, E., "Longitudinal Spin Seebeck Effect Free from the Proximity Nernst Effect," Phys. Rev. Lett. **110**(6), 67207 (2013).

[16] Jourdan, M., Minár, J., Braun, J., Kronenberg, A., Chadov, S., Balke, B., Gloskovskii, A., Kolbe, M., Elmers, H. J., et al., "Direct observation of half-metallicity in the Heusler compound Co2MnSi," Nat. Commun. **5**, 3974 (2014).

[17] Pfeiffer, A., Hu, S., Reeve, R. M., Kronenberg, A., Jourdan, M., Kimura, T.., Kläui, M., "Spin currents injected electrically and thermally from highly spin polarized Co2MnSi," Appl. Phys. Lett. **107**(8), 82401 (2015).

[18] Sakuraba, Y., Nakata, J., Oogane, M., Kubota, H., Ando, Y., Sakuma, A.., Miyazaki, T., "Huge spin-polarization of L21-ordered Co2MnSi epitaxial heusler alloy film," Japanese J. Appl. Physics, **44**(33–36) (2005).

[19] Nedelkoski, Z., Hasnip, P. J., Sanchez, A. M., Kuerbanjiang, B., Higgins, E., Oogane, M., Hirohata, A., Bell, G. R.., Lazarov, V. K., "The effect of atomic structure on interface spin-polarization of half-metallic spin valves: Co2MnSi/Ag epitaxial interfaces," Appl. Phys. Lett. **107**(21), 212404 (2015).

[20] Geiersbach, U., Bergmann, A.., Westerholt, K., "Preparation and structural properties of thin films and multilayers of the Heusler compounds Cu 2 MnAl , Co 2 MnSn , Co 2 MnSi and Co 2 MnGe," Thin Solid Films **425**, 225–232 (2003).

[21] Gercsi, Z., Rajanikanth, a., Takahashi, Y. K., Hono, K., Kikuchi, M., Tezuka, N.., Inomata, K., "Spin polarization of Co 2FeSi full-heusler alloy and tunneling magnetoresistance of its magnetic tunneling junctions," Appl. Phys. Lett. **89**(8), 082512 (2006).

[22] Oksenenko, V. A., Kulagin, V. A., Kudryavtsev, Y. V., Dubowik, J., Gościańska, I.., Troshchenkov, Y. N., "Magnetic properties of Co2MnGa Heusler alloy films with different crystalline order," J. Magn. Magn. Mater. **316**(2), 407–410 (2007).

[23] Pai, C. F., Liu, L., Li, Y., Tseng, H. W., Ralph, D. C.., Buhrman, R. A., "Spin transfer torque devices utilizing the giant spin Hall effect of tungsten," Appl. Phys. Lett. **101**(12), 122404 (2012).

[24] Liu, L., Pai, C.-F., Li, Y., Tseng, H. W., Ralph, D. C.., Buhrman, R. A., "Spin-Torque Switching with the Giant Spin Hall Effect of Tantalum," Science (80-.). **336**(6081), 555–558 (2012).

[25] Ramos, R., Kikkawa, T., Aguirre, M. H., Lucas, I., Anadón, A., Oyake, T., Uchida, K., Adachi, H., Shiomi, J., et al., "Unconventional scaling and significant enhancement of the spin Seebeck effect in multilayers," Phys. Rev. B **92**(22), 220407 (2015).

[26] Lee, K.-D., Kim, D.-J., Yeon Lee, H., Kim, S.-H., Lee, J.-H., Lee, K.-M., Jeong, J.-R., Lee, K.-S., Song, H.-S., et al., "Thermoelectric Signal Enhancement by Reconciling the Spin Seebeck and Anomalous Nernst Effects in Ferromagnet/Non-magnet Multilayers," Sci. Rep. **5**(1), 10249 (2015).

[27] Uemura, T., Imai, Y., Kawagishi, S., Matsuda, K.., Yamamoto, M., "Epitaxial growth and characterization of Co2MnSi thin films on GaAs with MgO interlayer," Phys. E Low-dimensional Syst. Nanostructures **40**(6), 2025–2027 (2008).

[28] Singh, L. J., Barber, Z. H., Kohn, A., Petford-Long, A. K., Miyoshi, Y., Bugoslavsky, Y.., Cohen, L. F., "Interface effects in highly oriented films of the Heusler alloy Co 2MnSi on GaAs(001)," J. Appl. Phys. **99**(1), 013904 (2006).

[29] Wang, W. H., Przybylski, M., Kuch, W., Chelaru, L. I., Wang, J., Lu, Y. F., Barthel, J.., Kirschner, J., "Spin polarization of single-crystalline Co2MnSi films grown by PLD on GaAs(001)," J. Magn. Magn. Mater. **286**, 336–339 (2005).

[30] Wang, W., Przybylski, M., Kuch, W., Chelaru, L., Wang, J., Lu, Y., Barthel, J., Meyerheim, H.., Kirschner, J., "Magnetic properties and spin polarization of Co2MnSi Heusler alloy thin films epitaxially grown on GaAs(001)," Phys. Rev. B **71**(14), 144416 (2005).

[31] Branford, W. R., Singh, L. J., Barber, Z. H., Kohn, A., Petford-Long, A. K., Roy, W. Van., Magnus, F., Morrison, K., Clowes, S. K., et al., "Temperature insensitivity of the spin-polarization in Co 2 MnSi films on GaAs (001)," New J. Phys. **9**(2), 42–42 (2007).

[32] Ueda, K., Nishiwaki, M., Soumiya, T.., Asano, H., "Fabrication of epitaxial Co2MnSi films on lattice-matched MgAl2O4 substrates by ion-beam assisted sputtering," Thin Solid Films **570**, 134–137 (2014).

[33] Matsushita, N., Takamura, Y., Fujino, Y., Sonobe, Y.., Nakagawa, S., "Magnetic anisotropy of [Co 2 MnSi/Pd] n superlattice films prepared on MgO(001), (110), and (111) substrates," Appl. Phys. Lett. **106**(6), 62403 (2015).

[34] Liu, H., Honda, Y., Taira, T., Matsuda, K., Arita, M., Uemura, T.., Yamamoto, M., "Giant tunneling magnetoresistance in epitaxial Co 2 MnSi/MgO/Co 2 MnSi magnetic tunnel junctions by half-metallicity of Co 2 MnSi and coherent tunneling," Appl. Phys. Lett. **101**(13), 132418 (2012).

[35] Cox, C., Caruana, A. J., Cropper, M. D., Kinane, C., Charlton, T. R.., Morrison, K., "Growth and Optimisation of polycrystalline Co2MnSi thin films on amorphous substrate SiO2," Preprint (2017).

[36] Webster, P. J., "Magnetic and chemical order in Heusler alloys containing cobalt and manganese," J. Phys. Chem. Solids **32**(6), 1221–1231 (1971).

[37] Sola, A., Bougiatioti, P., Kuepferling, M., Meier, D., Reiss, G., Pasquale, M., Kuschel, T.., Basso, V., "Longitudinal spin Seebeck coefficient: heat flux vs. temperature difference method," Sci. Rep. **7**, 46752 (2017).

[38] Liu, Y., Shelford, L. R., Kruglyak, V. V., Hicken, R. J., Sakuraba, Y., Oogane, M.., Ando, Y., "Optically induced magnetization dynamics and variation of damping parameter in epitaxial Co2 MnSi Heusler alloy films," Phys. Rev. B - Condens. Matter Mater. Phys. **81**(9), 094402 (2010).

[39] Schneider, H., Vilanova, E., Balke, B., Felser, C.., Jakob, G., "Hall effect in laser ablated Co_2(Mn,Fe)Si thin films," J. Phys. D. Appl. Phys. **42**(8), 084012 (2009).

[40] Gaier, O., Hamrle, J., Hermsdoerfer, S. J., Schulthei?, H., Hillebrands, B., Sakuraba, Y., Oogane, M.., Ando, Y., "Influence of the L21 ordering degree on the magnetic properties of Co2MnSi Heusler films," J. Appl. Phys. **103**(10), 103910 (2008).

[41] Ritchie, L., Xiao, G., Ji, Y., Chen, T., Chien, C., Zhang, M., Chen, J., Liu, Z., Wu, G., et al., "Magnetic, structural, and transport properties of the Heusler alloys Co2MnSi and NiMnSb," Phys. Rev. B **68**(10), 104430 (2003).

[42] Kämmerer, S., "The Heusler alloy Co2MnSi in thin films," Univ. Bielefeld (2004).

[43] Comtesse, D., Geisler, B., Entel, P., Kratzer, P.., Szunyogh, L., "First-principles study of spin-dependent thermoelectric properties of half-metallic Heusler thin films between platinum leads," Phys. Rev. B - Condens. Matter Mater. Phys. **89**(9), 094410 (2014).